Liquid Crystals
Publication details, including instructions for authors and subscription information:
http://www.informaworld.com/smpp/title~content=t713926090

Modelling zenithal bistability at an isolated edge in nematic liquid crystal cells

C. Uche[a]; S. J. Elston[a]; L. A. Parry-Jones[a]
[a] Department of Engineering Science, University of Oxford, Oxford OX1 3PJ, United Kingdom

To cite this Article Uche, C. , Elston, S. J. and Parry-Jones, L. A.(2006) 'Modelling zenithal bistability at an isolated edge in nematic liquid crystal cells', Liquid Crystals, 33: 6, 697 — 704
To link to this Article: DOI: 10.1080/02678290600681997
URL: http://dx.doi.org/10.1080/02678290600681997

Liquid Crystals, Vol. 33, No. 6, June 2006, 697–704

Modelling zenithal bistability at an isolated edge in nematic liquid crystal cells

C. UCHE, S.J. ELSTON* and L.A. PARRY-JONES
Department of Engineering Science, University of Oxford, Parks Road, Oxford OX1 3PJ, United Kingdom

(*Received 14 July 2004; in final form 1 February 2006; accepted 2 February 2006*)

In recent experiments we observed bistable switching in devices made with long pitch square gratings on one surface. It was also discovered that the switching in these devices was localized mainly at isolated edges of the square grating profile. In this paper we present an initial study of surface-induced director configurations at isolated edges of a square profile in the absence of an applied voltage. Our emphasis is on understanding the effect of edge features such as the edge depth and edge inclination in forming stable high and low pre-tilt states. Models based on a Landau–de Gennes approach were used and solutions were found through numerical simulation using finite element methods; optical response was determined, based on wide angle beam propagation methods. Results from real cells are also presented. Our results show that static defect-stabilized states exist for a range of isolated edge depths and inclination angles. In particular, a combination of deep edge depths and steep edge inclinations produce stable high and low pre-tilt director configurations.

1. Introduction

Size, weight and power consumption of display systems have become crucial issues in today's consumer electronics, notably in mobile communication systems (e.g. mobile phones) and other applications such as PDAs and flat screen televisions, most of which use liquid crystal display (LCD) technology. Efficient liquid crystal displays are therefore required to reduce power consumption in order to build compact systems with smaller power supplies.

Consequently there is currently much research into the development of highly efficient (mostly nematic) bistable liquid crystal displays. One of the promising technologies is the zenithal bistable nematic device (ZBD) technology [1–3], where electro-optic bistability is achieved by the interaction of the liquid crystal director with an underlying grating structure. The actual switching process is thought to involve the production and annihilation of defects by the deformation of the average local orientation unit vector (**n** director). An example of a surface relief grating that might stabilize two zenithally bistable states is shown in figure 1. Zenithal bistable displays can store an image in the absence of switching voltages, and energy is only required to switch between the two states, making them suitable for passive addressing. This eliminates the need for expensive thin film transistors (TFTs) leading to low cost, low power and rugged displays. Prototype displays have been made with good optical performance and contrast ratios in the region of 25:1 [3].

A key task in optimizing zenithal bistable displays is to understand the exact role of the grating features (shape, height, etc.) in forming switchable states. Previous work was carried out on the study of grating-induced defects [4]. Nevertheless, there is still limited knowledge in this area and the effective prediction of real device characteristics is still elusive.

2. Basis of work

The electro-optic response of cells exhibiting zenithal bistability is a complex combination of the diffractive effects (due to the periodicity of the structure), back reflections and the bulk deformation of the director due to the underlying grating – this effect predominates. An understanding of the key influencing features of the grating will be instrumental in developing devices with consistent electro-optic properties. There is also the need to explore the effect of different grating shapes, e.g. square gratings, triangular gratings, etc. in producing bistable devices.

Periodic sinusoidal (or distorted sinusoidal) gratings have been used to produce bistable devices [1–3]. In such devices two homogeneous states occur, namely (i) a defect-free *high pre-tilt state* and (ii) a defect state also known as the *low pre-tilt state*. However we recently

*Corresponding author. Email: steve.elston@eng.ox.ac.uk

Liquid Crystals
ISSN 0267-8292 print/ISSN 1366-5855 online © 2006 Taylor & Francis
http://www.tandf.co.uk/journals
DOI: 10.1080/02678290600681997

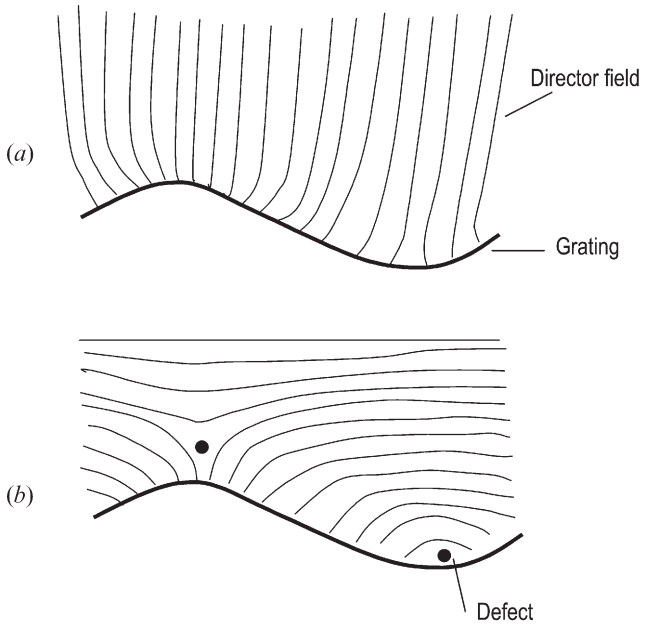

Figure 1. Zenithal bistable states due to a sinusoidal grating.

observed the switching in an interesting 5 µm thick test cell between crossed polarizers, see figure 2 (*a*). This cell was made with a long pitch square grating and results showed that this structure supports bistable switching mainly at the grating edges, in a region of approximately 3 µm around the edges, see figure 2 (*b*). This effect was observed when the square edges were at distances of greater than 5 µm from each other.

This observation prompted further investigation; hence the work outlined in this paper investigates the formation of high and low pre-tilt states at isolated edges in the absence of an applied voltage. This study can be extended for predicting the influence of periodic gratings of various shapes in producing zenithal bistability. The study of isolated edges involved both device modelling and experiments with test cells filled with E7 liquid crystal (Merck). E7 is a eutectic mixture of four different cyanobiphenyl and cyanotriphenyl compounds with a positive dielectric anisotropy and nematic-to-isotropic transition at 61°C.

3. General theory

An understanding of the director profiles within a cell is the key to understanding its electro-optic properties. This in turn depends on a combination of different energies as given by equation (1). The stable director configurations are those that minimize the total energy (F_{tot}). The total energy F_{tot} is a combination of elastic, surface, electromagnetic and thermotropic energies, as given by:

$$F_{\text{tot}} = F_{\text{elastic}} + F_{\text{surface}} + F_{\text{electromagnetic}} + F_{\text{thermotropic}}. \quad (1)$$

Using the Landau–de Gennes approach the total energy (F_{tot}) can be defined in terms of a 3×3 traceless Q-tensor with five independent elements, where q_i are the Q-tensor elements for $i=1\ldots5$; this can be written as:

$$\mathbf{Q} = \begin{Bmatrix} q_1 & q_2 & q_3 \\ q_2 & q_4 & q_5 \\ q_3 & q_5 & -q_1 - q_4 \end{Bmatrix} \quad (2a)$$

which in the uniaxial limit can be expressed as:

$$\mathbf{Q}_{\text{uniaxial}} = S\left(n_j n_k - \frac{\delta_{jk}}{3}\right) \quad (2b)$$

where S is the order parameter and j, k are indices. The Q-tensor approach was used to allow for changes in the order parameter and to ensure the equivalence of the **n** and –**n** orientations of the liquid crystal director. In general it can be biaxial, although it reduces to the uniaxial limit in regions away from defects.

Each of the energies in equation (1) will be briefly discussed in the following sections; we will also highlight which energies are used in this work as well as the assumptions made.

3.1. *Elastic energy*

The liquid crystal director field undergoes three main distortions, namely splay, twist and bend, and in the more conventional Frank notation the energies of these depend on three elastic constants K_{11}, K_{22}, K_{33}, respectively. These elastic energies are combined to form the Frank–Oseen equation [5]. We used the one-constant approximation where $K_{11}=K_{22}=K_{33}=K$, and in Q-tensor form this is given as:

$$F_{\text{elastic}} = \frac{L}{4}\frac{\partial Q_{ij}}{\partial_{x_k}}\frac{\partial Q_{ij}}{\partial_{x_k}} \quad (3)$$

where i, j, k are indices. The choice of $L/4$ as the pre-factor ensures that in the limit of perfectly uniaxial liquid crystal materials (i.e. the uniaxial order parameter $S=1$) we have $K=L$. More generally we can write $K=LS^2$. In addition there should in principle be a term associated with saddle-splay (the K_{24} term in the Frank notation). However, as is common in the one constant approximation, we set $K_{24}=0$. (This is reasonable because the term transforms into the boundary condition and other bulk terms already included.)

3.2. *Surface energy*

For a liquid crystal confined within a device the anchoring strength for the on-surface molecules

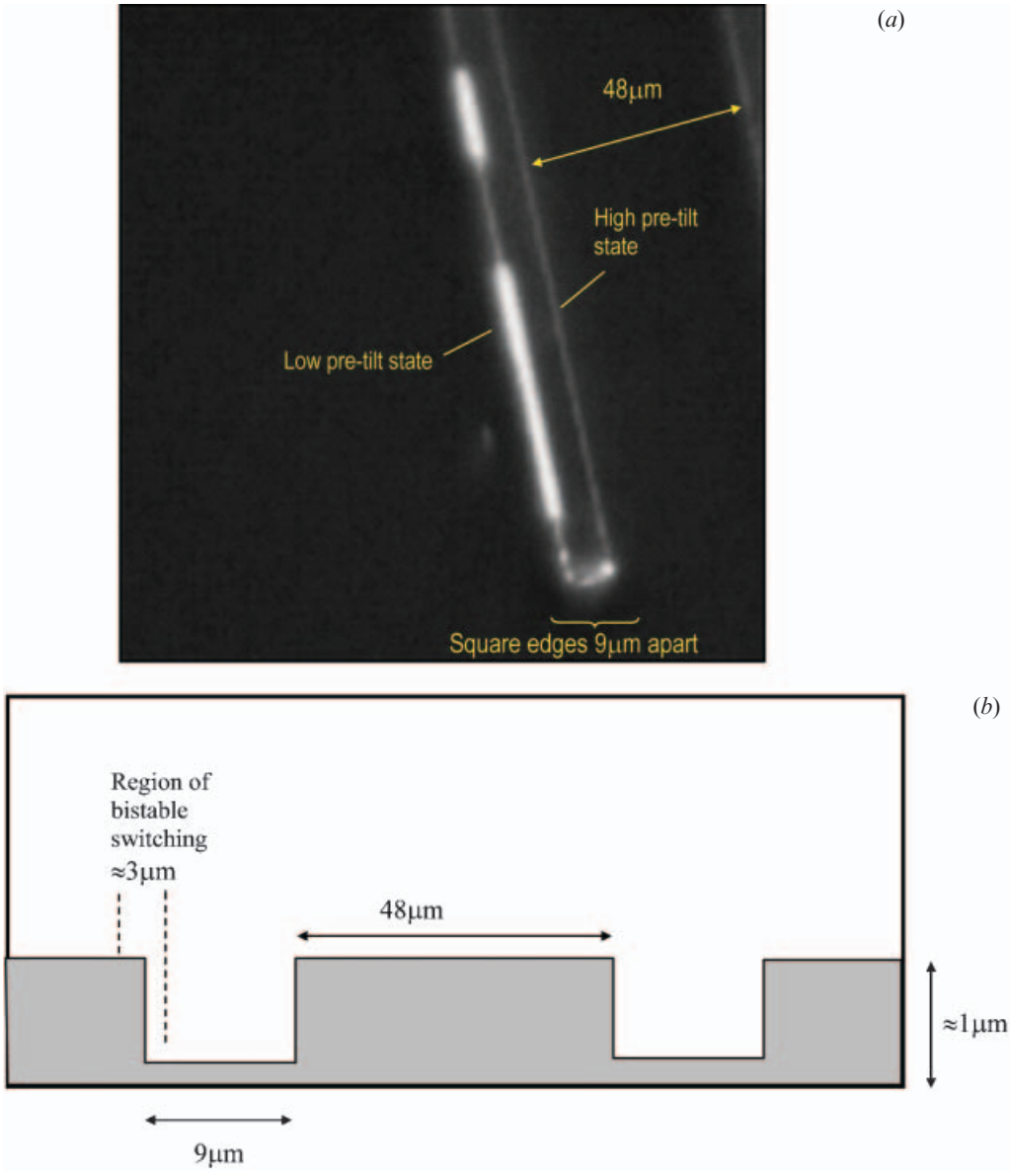

Figure 2. (*a*) Bistable switching of a 5 μm thick cell showing intensities of a low pre-tilt and high pre-tilt states; (*b*) the profile of the grating used in the device.

depends on the alignment material and the form of alignment—homeotropic, homogenous, tilted, etc. For a small deviation of the surface director the surface anchoring energy is conventionally expressed by the Rapini–Papoular equation [6]. A similar form can be used in Q-tensor notation and can be expressed as $F_{\text{surface}} = \frac{W}{2}\text{tr}\left(\mathbf{Q}|_s - \mathbf{Q}_s\right)^2$ where W is the anchoring strength, $\mathbf{Q}|_s$ is the Q-tensor value at the surface, $\mathbf{Q}_s$ is the Q-tensor value preferred by the surface due to alignment, etc. In this work we have assumed a strong anchoring and therefore use the limit $W \to \infty$ in our model. This leads to the reasonable approximation $\mathbf{Q}|_s = \mathbf{Q}_s$ with the on-the-surface director orientation defined as the surface normal.

3.3. *Electromagnetic energy*

This results both from externally applied electrical fields and from internal fields. We do not deal here with externally applied electric fields. However, variations in Q-tensor values might nevertheless be relevant. This is most easy to understand by considering how variation in the orientation of the **n**-director and variation in the magnitude of the scalar order parameter S give rise to

flexoelectricity and order electricity respectively [7]. In the Q-tensor notation these two effects are fundamentally coupled. They lead to internal fields that can couple both to flexoelectricity/order electricity, and to the dielectric anisotropy of the liquid crystal material.

However, for our application, the flexoelectricty and order electricity will be considered negligible due to the screening effect of ions within the liquid crystal material. Estimation of the effective field due to these effects (based on typical flexoelectric coefficients of around $10^{-11}\,\mathrm{Cm}^{-1}$) indicates that it is rather small. It is therefore reasonable to assume that in the static state the bulk flexoelectric effect is screened by the ions present in the mesophase, and at surfaces it is screened due to selective ion absorption at a substrate–nematic interface. Therefore there is no need to include flexoelectricity/order electricity or the dielectric anisotropy in our model, and hence the electromagnetic energy terms are not used in the work presented here.

3.4. *Thermotropic energy*

This energy is temperature dependent and defines the state of the liquid crystal, i.e uniaxial, biaxial or isotropic. The simplest form is a Taylor expansion about $\mathbf{Q}=0$ which can be written:

$$F_{\text{thermotropic}} = \frac{a}{2}\mathrm{tr}(\mathbf{Q}^2) + \frac{b}{3}\mathrm{tr}(\mathbf{Q}^3) + \frac{c}{2}\mathrm{tr}(\mathbf{Q}^4) \quad (4)$$

where a,b and c are the coefficients of the Landau expansion of thermotropic energy density and $\mathbf{Q}$ is the 3×3 traceless Q-tensor. The coefficients are normally temperature dependent but it can be assumed that b and c are independent of temperature whilst $a=\alpha(T-T^*)$, where $\alpha>0$ and T^* is the fixed temperature below which the isotropic state becomes unstable. These terms are included in our model.

4. Numerical model of director configurations at an isolated edge

Our analysis of isolated edge-induced deformation is based on a two dimensional model. Although the solution is based on the Q-tensor method, it is most useful to visualize the structure in terms of the **n**-director, as shown in an arbitrary position in the xy-plane in figure 3. The y-direction is the direction of the propagating optical plane waves, ϕ is director inclination angle w.r.t. to the lower surface of the cell and G_{dep} is the isolated edge depth. Using the two-dimensional model as shown in figure 3, the director remains in the plane of the page. The solution for the static state configuration is found by minimizing equation (1). This minimization is undertaken in Q-tensor form using the Euler–Lagrange approach and in principle involves five equations for the components of $\mathbf{Q}$ as defined in equation 2 (a). However, our experimental observations have indicated that in the structures of interest the director remains in a single plane (the xy-plane in our notation). In terms of the Q-tensor we make the assumption that this means that one of the eigenvectors of $\mathbf{Q}$ lies along the z-axis, which leads to a 'director' lying within the xy-plane except at the centre of defects. In this case it is only necessary to solve for three of the components of the Q-tensor, q_1, q_2 and q_4 (which can alternatively be expressed as q_{xx}, q_{xy} and q_{yy}, respectively). There are therefore three Euler–Lagrange equations for our two-dimensional model given by:

$$\sum_{j=1}^{2} \frac{\partial}{\partial_{xj}}\left(\frac{\partial F_{\text{tot}}}{\partial q_{i,j}}\right) = \frac{\partial F_{\text{tot}}}{\partial q_i} \quad (5)$$

for $i=1$, 2, 4 where q_i are the components of the Q-tensor, $q_{i,j}=\partial q_i/\partial x_j$ and F_{tot} is the total energy. These three equations were solved using a finite element package (FlexPDE) and the solution which minimizes the total free energy defines the director configuration in the cell.

As noted above, strong surface anchoring was assumed at both liquid crystal – substrate interfaces, with the on-surface director angle defined as the surface normal and the order parameter set to its equilibrium value. Periodic boundary conditions were used in the x-direction, so that at the ends of the computational space ($x=0$ and $x=L_x$) the values of the Q-tensor are equal to one another.

4.1. *Isolated edge-induced static equilibrium states*

In the following text, the formation of high and low pretilt states by isolated grating edges in the absence of an applied voltage is investigated; this is a prelude to future models of bistable switching at these edges. Values of elastic and thermotropic constants, the parameters in equations (3) and (4), were $L=1.0\times10^{-11}\,\mathrm{N}$, $a=0.0$, $b=-3.0\times10^5$ and $c=5.0\times10^5$. These lead to elastic behaviour which is similar to that of a real material, an equilibrium uniaxial order parameter of $S=0.6$, and appropriate defect sizes. The isolated edge-induced effects were investigated in terms of edge depth (G_{dep}) and edge inclination (θ_{inc}). The parameters used in our simulations are shown in figure 3, where G_{dep} is the edge depth, h is the cell thickness, L_x is the width of the computational region and θ_{inc} is the inclination of the isolated edge. L_x is made sufficiently large (typically$>10\,\mu\mathrm{m}$) to ensure that the edge step behaves independently of other steps and therefore can be considered as an isolated feature. The assumption made was that the director has a strong anchoring and is the normal to both the edge surface profile and the upper

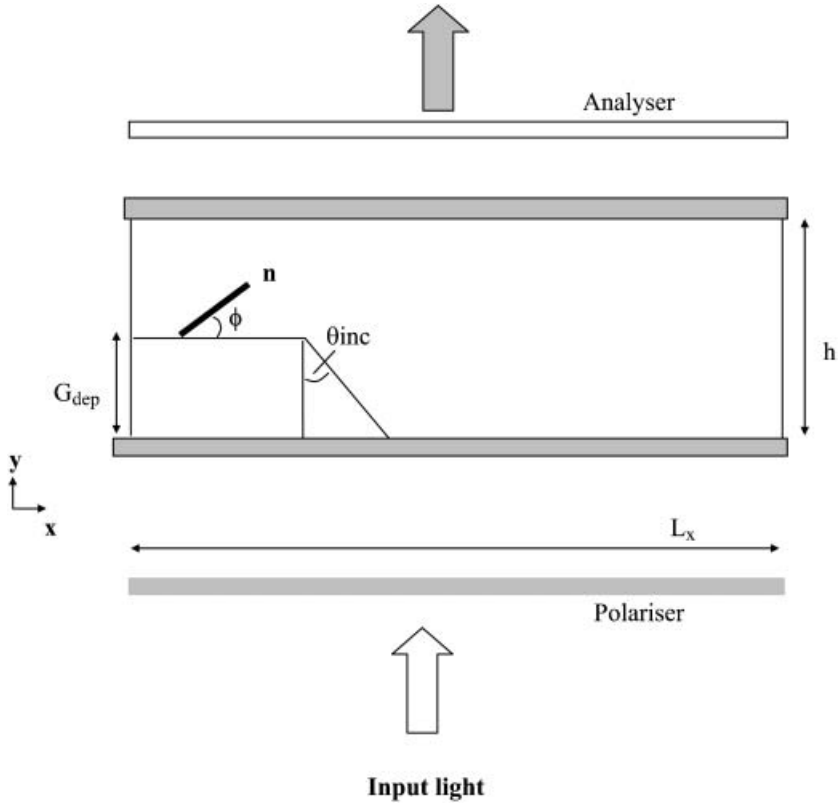

Figure 3. Isolated edge parameters for a two-dimensional model.

surface of the cell at all points; this results in a high pre-tilt (i.e. a non-defect state) in the absence of an edge induced deformation, as shown in figure 4 (*a*). The transmission due to the low pre-tilt, figure 4 (*b*), and high pre-tilt states correspond to the bright and dark states respectively (figure 2) since the local director deformation leads to an increase in the refractive index anisotropy experienced by the incoming light. figure 4 (*c*) shows a plot of the order parameter for the low pre-tilt (defect) state.

4.2. *Effect of changing the edge parameters*

A key interest is to gain insight into the relationship between edge depth (G_{dep}) and the formation of the low pre-tilt state. This effect was investigated using a cell model that is 5 μm thick. In the simulation, the edge depths were varied from 0.5 to 2 μm, for edge inclination angles (θ_{inc}) with values 0–60°, as shown in figure 5. All of the simulations involve edge depths somewhat smaller than the cell thickness. It may be interesting to consider the case when the step depth approaches the cell thickness, but this is less directly analogous to the zenithal bistability which is of commercial interest, and we therefore limit the study to cases where the fixed homeotropic surface is somewhat distant from the step. The results show that the minimization of the free energy produces bistable states (i.e. either high or low pre-tilt states) mostly for deep edges ($G_{dep} > 0.5\,\mu m$) with small edge inclination angles ($\theta inc < 25°$). For some of the G_{dep}–θ_{inc} combinations, the bulk director can be biased into either the low pre-tilt or high pre-tilt state. In our approach this is probed by using a range of initial uniform director orientations in the model and then allowing relaxation to an equilibrium state to take place. The use of a range of initial states allows us to examine whether the device is monostable (always relaxes into the same equilibrium state whatever the starting state) or bistable (relaxes into one of two equilibrium states depending on the starting state). For shallower edges, i.e. $G_{dep} < 0.5\,\mu m$, or those with large edge inclination angles ($\theta_{inc} \geqslant \approx 30°$), the director configuration at the isolated edge is monostable, forming only the high pre-tilt state regardless of the initial orientation.

We also investigated the transmission of the high and low pre-tilt states formed with different G_{dep} values. Since the high pre-tilt state has very low transmission,

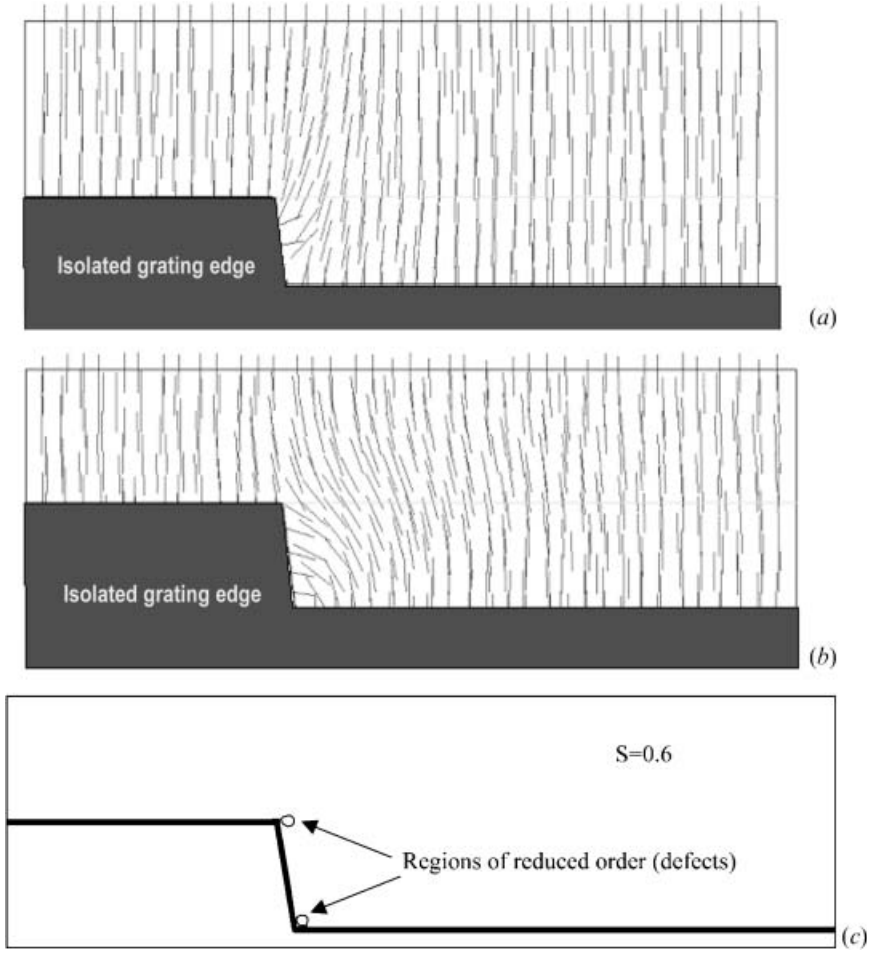

Figure 4. Numerical simulation of director configurations at an isolated edge showing (*a*) a high pre-tilt state, (*b*) a low pre-tilt state and (*c*) a plot of the order parameter for a low pre-tilt state. In (*c*) the bulk region has an equilibrium uniaxial order parameter of $S=0.6$. This is strongly suppressed in the vicinity of the defects at the edge corners. In the regions indicated the order is less than $S=0.4$. In the high-tilt state there remains a little suppression of order at the corners (due to the sharp changes in orientation).

only the transmission of the low pre-tilt states was plotted. A plot of the intensity of the low pre-tilt state for a fixed edge inclination ($\theta_{inc}=15^\circ$) is given in figure 6. The optical outputs (for the various director configurations) were obtained using a numerical wide angle beam propagation method (BPM) with the model sandwiched between crossed polarizers [8, 9].

Apart from the effect of G_{dep}, the diagram of figure 5 also shows that the range of edge inclination angles for the low pre-tilt state is approximately between 0 and 25°; this is the range of inclination angles (θ_{inc}) necessary for stabilizing the high energy low pre-tilt state. As in the case of the edge depth, it was of interest to determine the edge transmission over the 0–25° range. A plot of a 5 μm thick model transmission as a function of θ_{inc} (for $G_{dep}=2\,\mu m$) is shown in figure 7. We found that very low θ_{inc}, i.e. sharp edges, encourage the low pre-tilt state, whereas increased θ_{inc} ($\geqslant\approx 30^\circ$) encourages the high pre-tilt state, as might be expected from the physical geometry and the minimization of the energy. Hence in figure 7, as the inclination angle exceeds 30°, the edge can no longer support a low pre-tilt state—its collapse is marked by a fall in transmission at 60°. Hence the director configuration becomes monostable, supporting only the high pre-tilt state.

5. Conclusion

Numerical models based on a *Q*-tensor approach were used to study isolated edge-induced director configurations in nematic cells. The emphasis was on understanding the part played by the underlying edge features such as the edge depth (G_{dep}) and the edge inclination angle (θ_{inc}), with other factors such as surface anchoring fixed. For static states, our model shows that a combination of deep edge depths ($>0.5\,\mu m$) and very steep edge inclination angles leads to bistable devices,

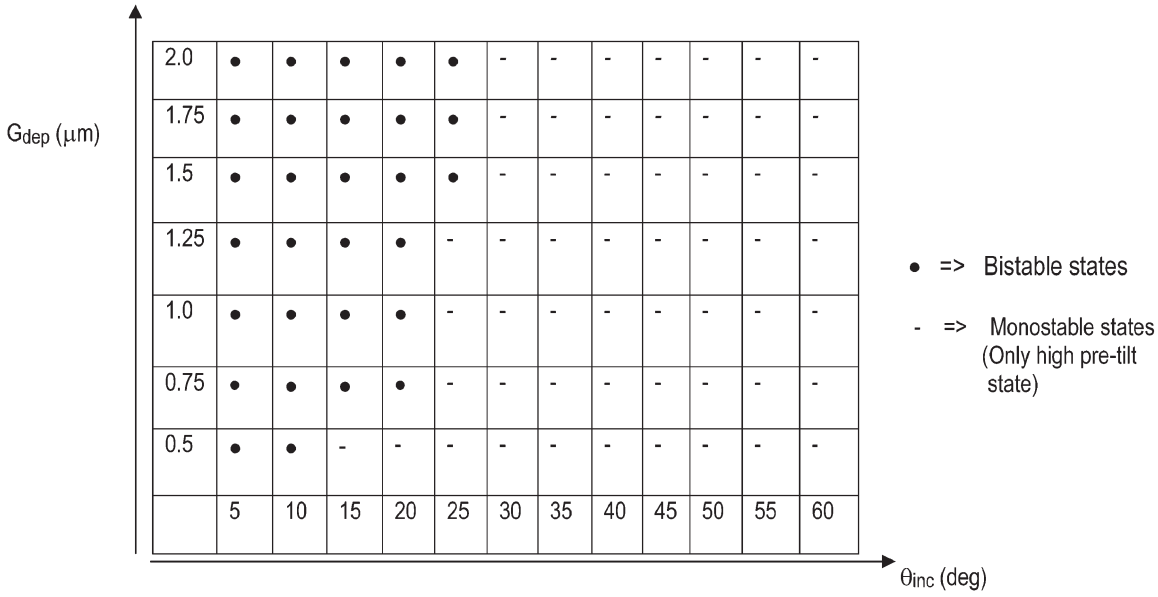

Figure 5. Numerical simulation of an isolated edge showing the formation of bistable states for deep edges with low edge inclination.

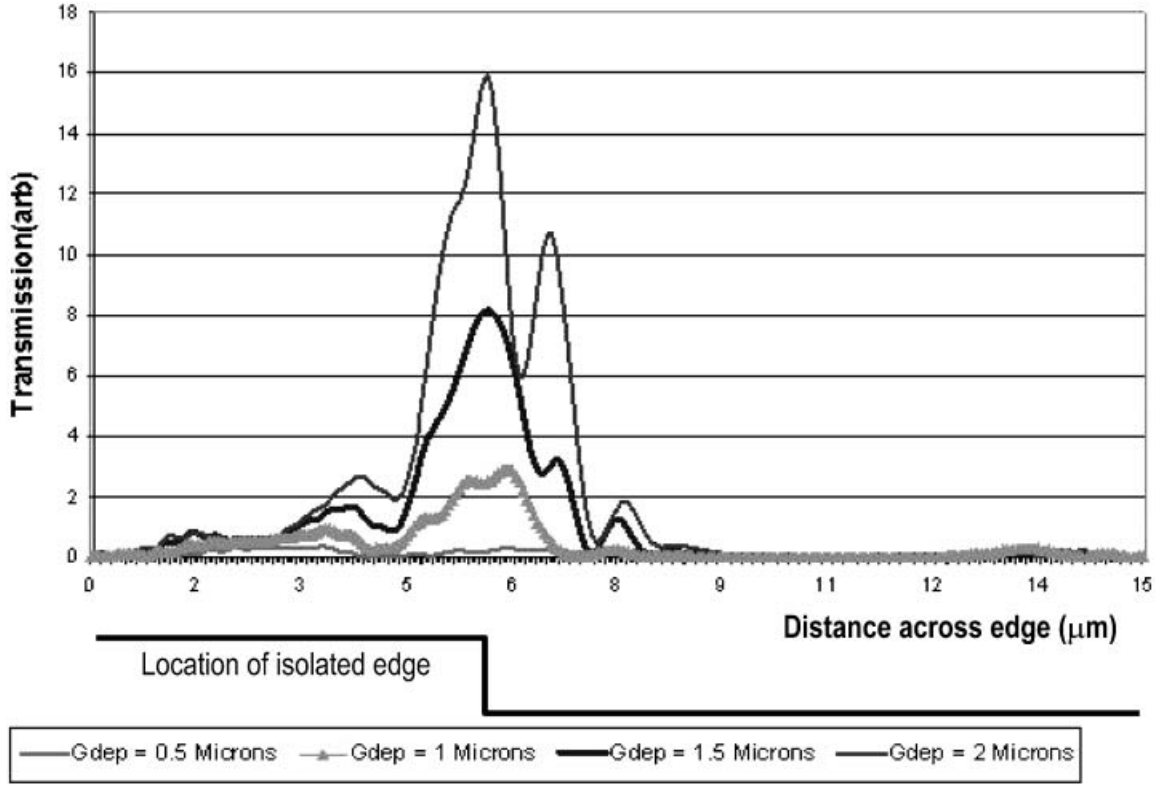

Figure 6. Numerical simulation showing the transmission in the vicinity of an isolated edge (in a low pre-tilt state) as a function of the distance across the edge for various edge depths (G_{dep}). For $G_{dep} \geqslant 0.5\,\mu m$ the director configuration is bistable and its low pre-tilt states show higher transmission, whereas the corresponding high pre-tilt states show lower transmission.

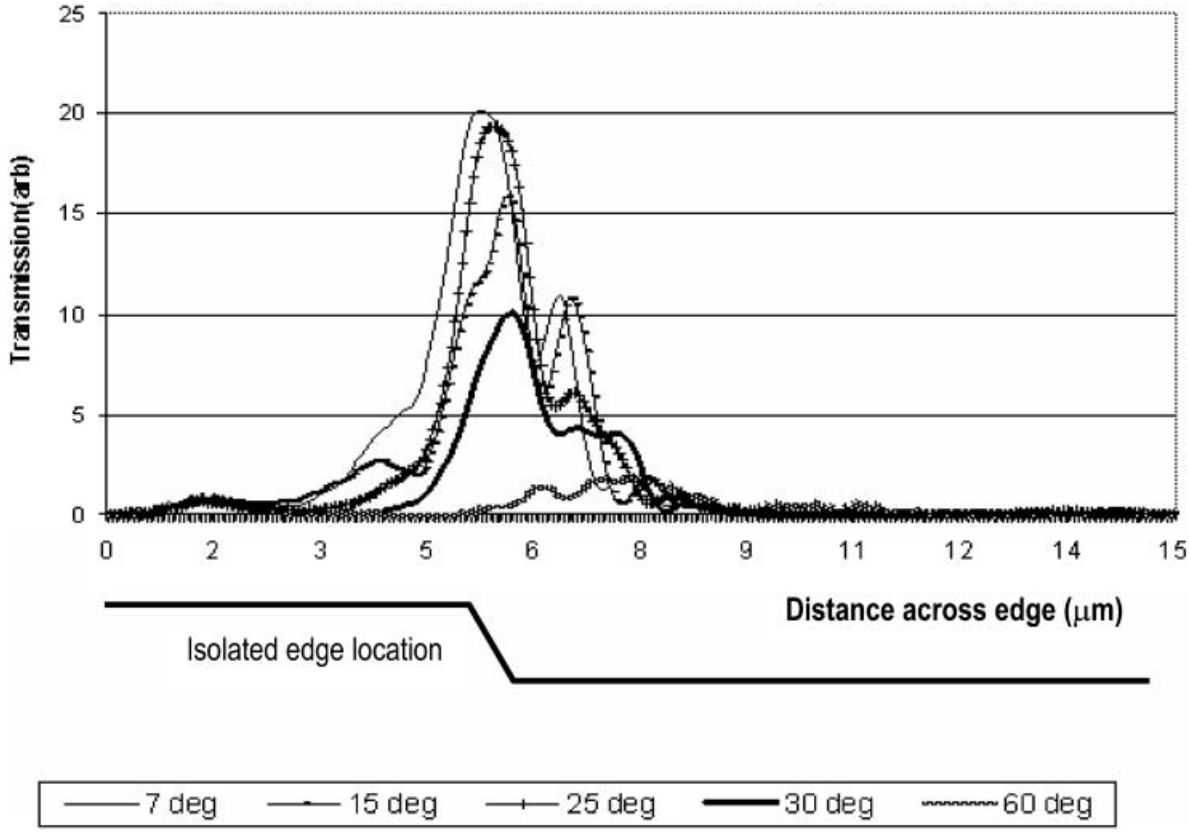

Figure 7. Numerical simulation of an isolated edge showing the effect of the edge inclination on transmission in the vicinity of the edge for the low pre-tilt state. At 60° the low pre-tilt state has collapsed hence the device is monostable, favouring only the high pre-tilt state.

i.e. those that readily form low and high pre-tilt states. The range of edge inclination angle for bistability is approximately 0–25°. Conversely, shallow edge depths and very high edge inclination angles produce only the high pre-tilt state. Results from the model show that with θ_{inc} greater than 30°, it is impossible to stabilize the high energy low pre-tilt state, regardless of the edge depth.

Other results show that the isolated edge transmission is strongly dependent on the various combinations of G_{dep} and θ_{inc} for producing bistable states. The plot of figure 6 indicates a strong correlation between G_{dep} and the isolated edge transmission for the low pre-tilt state, showing a sixteen-fold increase in the transmission (between crossed polarizers) as G_{dep} increases from 0.5 to 2 μm. Reduction of G_{dep} below 0.5 μm causes a collapse of the high energy low pre-tilt state. This indicates a transition from a bistable to a monostable director configuration, as only the high pre-tilt state can be formed. Future work will investigate switching between the high pre-tilt and low pre-tilt states, taking into account other factors such as edge smoothness and surface anchoring variations.

Acknowledgements

The authors wish to acknowledge useful discussions with Dr Carl Brown. The financial support of the EPSRC and the Royal Society is also gratefully acknowledged.

References

[1] G.P. Bryan-Brown, C.V. Brown, J.C. Jones, E.L. Wood, I.C. Sage, P. Brett, J. Rudin. *SID Dig.*, **XXXIII**, 37 (1997).
[2] J.C. Jones, J.R. Huges, A. Graham, P. Brett, G.P. Bryan-Brown, E.L. Wood. *IDW*, 301 (2000).
[3] E.L. Wood, P.J. Brett, G.P. Bryan-Brown, A. Graham, R.M. Amos, S. Beldon, E. Cubero, J.C. Jones. *Proc. SID 02*, 22 (2002).
[4] C.V. Brown, M.J. Towler, V.C. Hui, G.P. Bryan-Brown. *Liq. Cryst.*, **27**, 233 (2000).
[5] P.G. de Gennes, J. Prost. *The Physics of Liquid Crystals,* 2nd Edn, 102 (1993).
[6] A. Rapini, M.J. Papoular. *J. Physique Colloq.*, **30 (C4)**, 54 (1969).
[7] G. Barbero, G. Skacej, A.L. Alexe-Ionescu. *Phys. Rev. Lett.*, **56**, 2056 (1986).
[8] E.E. Kriezis, S.J. Elston. *J. Mod. Opt.*, **46**, 1201 (1999).
[9] E.E. Kriezis, S.J. Elston. *Opt. Commun.*, **165**, 99 (1999).